Original

Maier, P.; Mendis, C.; Tober, G.; Hort, N.:

Tailoring properties of cast Mg10Gd by alloying Nd and heat treatment

In: Emerging Materials Research (2013) ICE Publishing

DOI: 10.1680/emr.13.00021

Emerging Materials Research
Volume 2 Issue EMR5
Tailoring properties of cast Mg10Gd by alloying Nd and heat treatment
Maier, Mendis, Tober and Hort

ice | science

Pages 229–238 http://dx.doi.org/10.1680/emr.13.00021
Themed Issue Research Paper
Received 21/05/2013 Accepted 21/08/2013
Published online 24/08/2013
Keywords: alloys/corrosion/magnesium/material characterization/mechanical properties

ice Institution of Civil Engineers publishing

Tailoring properties of cast Mg10Gd by alloying Nd and heat treatment

Petra Maier Dr.-Ing.*
University of Applied Sciences Stralsund, Stralsund, Germany

Gerhard Tober MSc
University of Applied Sciences Stralsund, Stralsund, Germany

Chamini Mendis Dr.
Helmholtz-Zentrum Geesthacht, Geesthacht, Germany

Norbert Hort Dr.-Ing.
Helmholtz-Zentrum Geesthacht, Geesthacht, Germany

Magnesium-rare Earth alloys receive growing interest for medical applications as implant material due to their non-toxicity, high specific strength with moderate corrosion rate and elastic modulus comparable with bone. In this study, the corrosion properties of cast Mg10Gd modified with neodymium have been investigated by potentiodynamic measurements. Adding neodymium to Mg10Gd improves mechanical properties, but the influence on the corrosion behavior was rarely investigated. The heat treatment of Mg10Gd1Nd and Mg10Gd2Nd, especially T6, increased strength due to precipitation of prismatic plate precipitates. In most magnesium alloys, the degradation of α-Mg matrix preferentially due to the cathodic response of precipitates, the influence of type and distribution of the precipitates on the nature and dynamics of the corrosion process is discussed. The temperature increase from room to body temperature accelerates the corrosion processes. However, an extended repassivation is observed at higher temperatures.

1. Introduction

Degradable metallic materials, especially magnesium alloys, have increasingly become a focus of research interest during the past years.[1,2] The interest is based on the property profile of magnesium alloys, which is very close to that of human bone and the degradation behavior of the alloys.[3] The chemical composition and the processing route trigger the final microstructure and features of degradation. Gadolinium is a suitable alloying element for the design of magnesium implant alloys. Hort *et al*.[4] found that above 10 wt.% Gd precipitation hardening is observed in addition to the solute strengthening. Neodymium belongs to the group of rare earth elements with low solubility in magnesium and increases the strength due to precipitation while reducing the dendritic structure of the as-cast alloy. Hort *et al*. further showed that at 10 wt.% Gd, the corrosion rate is the lowest for the binary Mg-Gd alloys. The acute toxicity of gadolinium is only moderate, and the tests regarding the cytotoxicity in osteoblast-like cells showed that gadolinium could be a suitable alloying element for designing Mg-Gd-based implant materials for medical use[5].

The as-cast Mg10Gd*x*Nd (*x*–1 and 2 wt.%) alloys contain Mg_5(GdNd) particles that dissolve during solution heat treatment (T4).[6] During isothermal aging at 250°C (T6 heat treatment), plate-like precipitates form following the sequence described by Apps *et al*.[5] in Mg7Gd2Nd alloy. At the peak hardness, a mixture of β' (base-centered orthorhombic Mg_7Gd) and β_1 (fcc Mg_5Gd) phases were observed in Mg7Gd2Nd alloys.[6,7] The amounts of β' and β_1 phases are dependent on the ratio between gadolinium and neodymium.[6] Nishijima *et al*.[8] and He *et al*.[9] in their investigations on Mg 5at% Gd and Mg15Gd0·5Zr alloys, respectively, found that the microstructure in the peak-aged alloy was β' phase, while Vostry *et al*. reported that below 10 wt.% Gd in a binary alloy, the β' phase is absent in the peak-aged microstructures.[10]

The aim of this work is to study the effect of the amount of Nd, testing temperatures (22 and 37°C) and the heat treatments on the corrosion behavior of Mg10Gd*x*Nd alloys (where $x = 1$ and 2 wt.% Nd). Previous research by Maier *et al*.[11] on the influence of the microstructure on the passive/transpassive corrosion behavior of Mg10Gd base alloys has shown no significant difference between coarse dendritic grains and fine recrystallized grains. However, in that study, zero flow rate was applied, and thus, the pH value of the rather small amount of electrolyte increased significantly. Further research by Maier *et al*.[12] has shown that operating with a moving electrolyte (by applying adjustable flow rate) keeps the pH value around 8·5 and therefore provides a testing setup closer to reality in the human body environment, which may reveal the microstructural influences in a different light.

2. Materials and experimental procedure

Alloys investigated were prepared using the permanent mold direct chill casting technique[13,14] under a protective gas mixture

***Corresponding author e-mail address:** petra.maier@fh-stralsund.de

of argon and 2% sulfur hexafluoride at Helmholtz-Zentrum Geesthacht, Geesthacht, Germany. The casting temperature was 730°C, and the mild steel mold (inner surface has a thin boronitride coating) was preheated to 500°C. Gadolinium and neodymium were added as pure elements to the Mg melt before casting. The ternary alloys under investigation had nominal compositions of 10 wt.% Gd in addition to 1 and 2 wt.% Nd. In the Mg10Gd1Nd alloy, gadolinium and neodymium were present in the amounts of 8·13 and 0·74 wt.%. The actual composition of Mg10Gd2Nd is 9·17 wt.% Gd and 1·75 wt.% Nd. The binary alloy Mg10Gd was used for comparison and consists of 9·2 wt.% Gd. For the analysis of the overall chemical composition, inductively coupled plasma–optical emission spectroscopy was applied. The specimens were dissolved in concentrated nitric acid and diluted by a factor of 32 000. The alloys were solution treated (T4) at 525°C for 24 h and quenched into water at room temperature. The aging heat treatment (T6) was performed on these alloys at 250°C for 6 h to reach peak hardness based on previous investigations.[7] The mechanical properties were measured at room temperature using a Zwick 050 tensile testing machine (Germany) with an initial strain rate of 1×10^{-3} mms^{-1}, and a number of ten samples were tested for each alloy. An extensometer (Germany) is applied to determine the strength values. Elongation at fracture is determined by removing the fractured specimen from the grips, fitting the broken ends together and measuring the distance between gage marks. Tensile tests cannot be regarded as reliable methods for determining the Young's modulus of magnesium. It is known that the Young's modulus is influenced by the applied load, the composition and internal stresses. However, to get a rough guide, resonance frequency damping analysis method has been applied to determine the dynamic modulus of elasticity of the alloys in T4 condition, only. The microstructures of T6 heat-treated alloys were observed with a CM200 transmission electron microscope (Phillips,The Netherlands) operating at 200 kV, and the samples were prepared by twin jet electropolishing in 2% perchloric acid in methanol.

A three-electrode flow cell with a volume of 70 ml was used to evaluate polarization (current density–potential) curves using an Argenthal reference electrode. The measurement area at the working electrode was 150 mm^2. To prepare the surface of the samples for the corrosion tests, silicon carbide–grinding paper with a grit size of 1200 was used. Due to cleaning with ethanol and distilled water, drying and placing the sample in the cell 2 min have passed. The maximum flow rate possible by the applied pump, 8 l/min, was chosen to determine extreme conditions. As mentioned above, previous research[12] has shown that a moving electrolyte is necessary to keep the pH value around 8·5. A small volume of electrolyte leads to a strong increase in pH value, which is not the case in normal *in vivo* environments. Ringer acetate solution (1 l:6-g sodium chloride, 3·7-g sodium acetate, 0·134-g calcium chloride, 0·203-g magnesium chloride and 0·4-g potassium chloride; pH value of 6·5) was used as the corrosive media in this study due to its similarity to human blood. Results from this investigation are expected to be more practical for bioimplantation materials compared with 3% sodium chloride solution that is more aggressive. To force the magnesium alloy into strong anodic corrosion, the curve was traced from the negative potential end (–2000 mV) toward the positive end (+4000 mV). The key point of this measurement is to study the passive/transpassive behavior of Mg10Gd and its dependence on temperature, content of neodymium and heat treatment. The form of corrosion (selective, uniform or pitting corrosion) is evaluated by light optical microscopy and correlated to the voltammetric behavior. Since resulting pits, as a result of chemically damaged or not uniform passive films, appear in different shapes, that shape of pitting corrosion is of interest. According to ASTM-G46-94 'Guide for Examination and Evaluation of Pitting Corrosion', pits can become wide and shallow, elliptical, narrow and deep or undercut the surface. This is indentified through metallography where the corroded (pitted) sample is cross-sectioned to determine the pit shape and size as well as depth of penetration.

3. Results and discussion

3.1 Tensile properties and microstructures

Table 1 shows the tensile properties of as-cast (F), solution heat-treated (T4) and aged (T6) Mg10Gd*x*Nd alloys. A significant increase in the tensile yield strength (TYS) and ultimate tensile strength with T6 heat treatment is observed for both the 1 and 2 wt% neodymium-containing alloys. Such significant increment in strength was not apparent in a similarly heat-treated Mg10Gd alloy. An increase in the elongation at fracture is observed for the T4 heat-treated alloys. Mg10Gd1Nd-T4 shows the highest increase in elongation at fracture up to 7%. Independent of the alloy and heat treatment condition, all samples show brittle trans-granular fracture initiated from surface cracks or particles and pores in the inner. The Young's modulus is 43·71 ± 0·38 GPa, 44·22 ± 0·15 GPa and 44·45 ± 0·15 GPa for Mg10Gd, Mg10Gd1Nd and Mg10Gd2Nd in the T4 condition, respectively. No significant difference between the as-cast and heat-treated alloys is expected based on the findings of Hort *et al.*,[4] where four binary Mg-Gd alloys showed more or less the same values for E. Due to the increase in strength, the neodymium-containing alloys subjected to T4 and T6 heat treatments form the basis of the corrosion study. From the mechanical properties point of view, Mg10Gd1Nd-T4 shows the best combination of strength and ductility.

The microstructures of the as-cast conditions, see Figure 1(a) for Mg10Gd1Nd as a representative example, show a coarse columnar structure with a grain size up to 500 μm in size. These columnar grains are characterized by dendrite arms with preferred

Condition	Tensile property	Mg10Gd	Mg10Gd1Nd	Mg10Gd2Nd
F	TYS (MPa)	86·6 ± 9·8	114·5 ± 3·8	117·6 ± 3·5
	UTS (MPa)	131·2 ± 15·8	162·4 ± 7·8	160·2 ± 6·2
	Elongation at fracture (%)	2·5 ± 0·6	2·5 ± 0·5	1·2 ± 0·4
T4	TYS (MPa)	68·7 ± 2·4	108·3 ± 3·4	106·4 ± 5·8
	UTS (MPa)	111·7 ± 9·3	174·4 ± 0·8	162·1 ± 5·8
	Elongation at fracture (%)	3·2 ± 0·5	7·0 ± 1·2	2·9 ± 0·4
T6	TYS (MPa)	87·6 ± 3·8	164·3 ± 3·0	176·6 ± 3·4
	UTS (MPa)	132·3 ± 7·4	257·2 ± 5·2	224·6 ± 5·2
	Elongation at fracture (%)	2·2 ± 0·6	3·0 ± 0·9	0·8 ± 0·2

TYS, tensile yield strength; UTS, ultimate tensile strength.

Table 1. Tensile properties in F, T4 and T6 conditions.

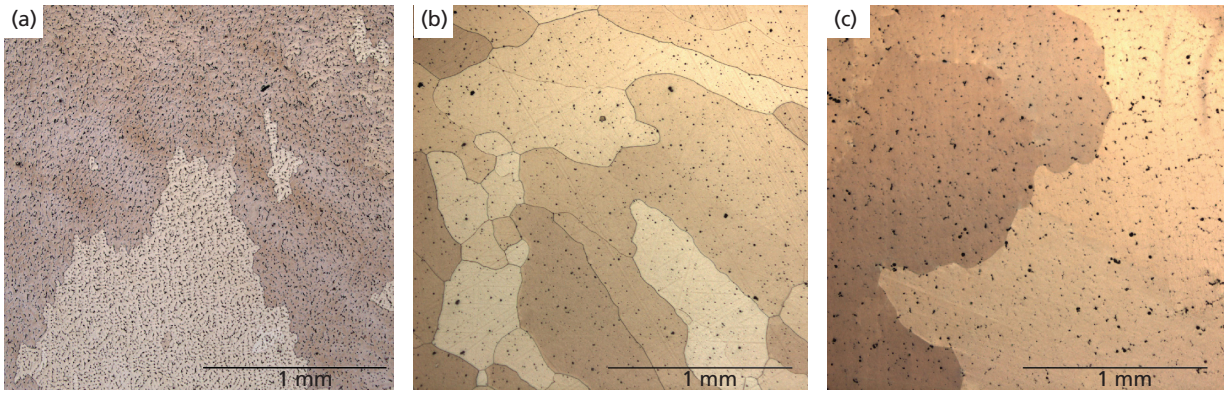

Figure 1. Micrographs of Mg10Gd1Nd: (a) as-cast Mg10Gd1Nd reveals dendritic coarse columnar microstructure. (b) T4 and (c) T6 reveal disappearance of dendritic microstructure during heat treatment.

orientation direction as induced by the directional solidification. Figure 1(b) (solution annealing) and Figure 1(c) (age hardening) present that during heat treatment the dendritic microstructure disappears.

The transmission electron microscopy images of T6 heat-treated alloys are shown in Figure 2. The Mg10Gd1Nd alloy contains a coarse distribution of β_1 phase (see Figure 2(a)), while the increase in the neodymium content to 2 wt.% resulted in a duplex microstructure of coarse β_1-phase precipitates (Mg_5Gd) and regions containing much finer precipitates β' (Mg_7Gd), Figure 2b. The fine-scale precipitates observed in the microstructures of Mg10Gd2Nd were identified as β' phase using electron microdiffraction (not shown here). On the basis of the previous investigations by Vostry *et al.*,[9] it is proposed that with increased addition of neodymium, a fine distribution of β'-phase precipitates was stabilized at the peak hardness leading to an increase in the yield strength.

After T6 heat treatment, the number density of $2{\cdot}9 \times 10^{-19}$ m^{-3} was calculated for the coarse particles in Mg10Gd1Nd and $2{\cdot}5 \times 10^{-19}$ m^{-3} in Mg10Gd2Nd. The number density of fine precipitates in Mg10Gd2Nd after T6 is $1{\cdot}2 \times 10^{-20}$ m^{-3}, but the contribution is not uniform. The coarse precipitates found in T6 condition are not observed in T4, and no particles have been found.

Microgalvanic corrosion is driven by the difference in electrochemical potential between intermetallics and the matrix. The presence of intermetallic particles changes the composition of the matrix material. The composition of the matrix material surrounding the particles has not been measured yet but will contain less gadolinium and neodymium. Investigations on the nanohardness of particles, surrounding matrix and solid solution have shown less hardness in matrix-surrounding material[15]. This depleted region of alloying elements underlines the different Mg-Gd-Nd ratio. However, not only the chemical composition

of particle surrounding material is of interest but also its local electrochemical potential.

3.2 Influence of test temperature (22/37°C)

It is known that increasing the test temperature increases the microgalvanic corrosion[16]. Figure 3(a) shows that for 22°C, the passive oxide film is not stable; a constant increase of corrosion current was observed for Mg10Gd2Nd in T4 condition. Only at a very high potential (3500 mV), the corrosion current is kept at a constant current density (45 mV/cm^2), followed by ongoing breakdown and re-passivation.

Figure 4(a) shows the microstructure with strong corrosion attack after potentiodynamic test. This micrograph also shows that the grain boundary acts as the cathodic area and withstands the ongoing corrosion, and the areas away from the grain boundary show significant erosion (250 µm deeper than remained grain

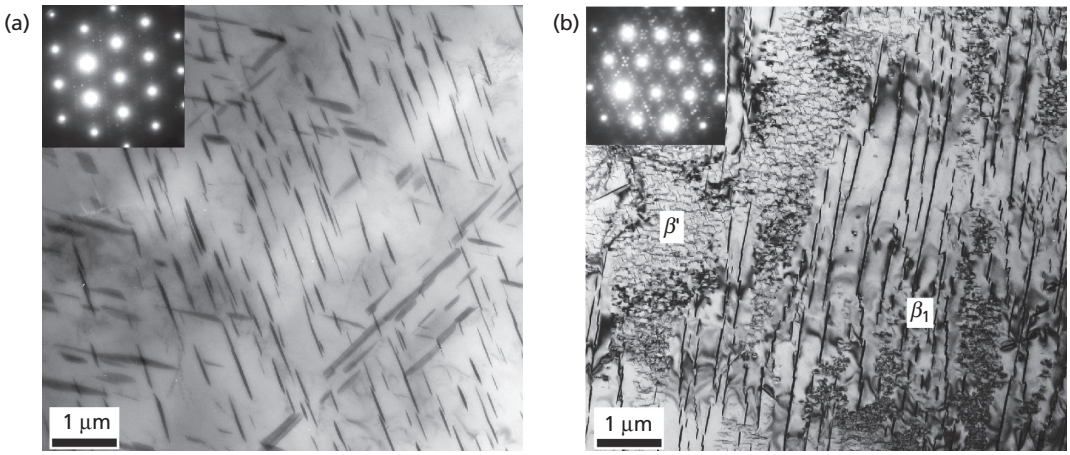

Figure 2. TEM micrographs of Mg10GdxNd-T6: (a) 1Nd containing only β_1 phase (b) 2Nd containing β_1 and β' phases. β_1 is fcc Mg_5Gd and β' is base-centered orthorhombic Mg_7Gd. TEM, transmission electron microscopy.

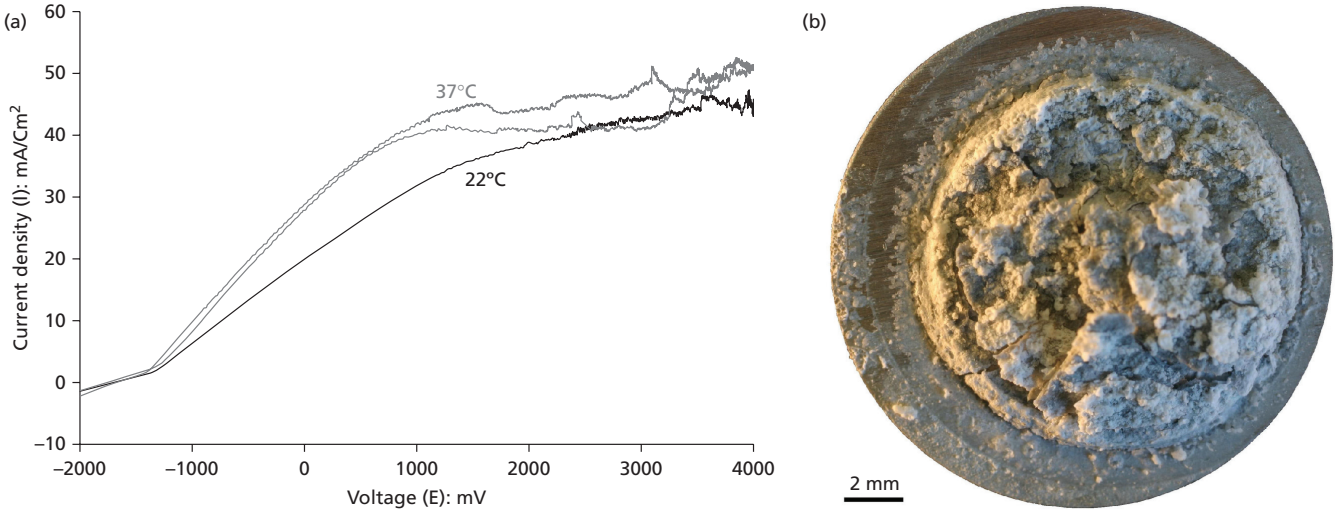

Figure 3. Potentiodynamic polarization curves (current density–potential (I–E) curves) of (a) Mg10Gd2Nd in T4 condition and (b) corroded surface of Mg10Gd2Nd in T4 condition after passing breakdown potential (tested at 37°C to 4000 mV). Gray: 37°C, black: 22°C.

boundary). Scanning the cross-sectioned micrograph along the corroded surface, pitting corrosion is observed. The pits are shaped wide and shallow with a size of up to 50-µm width and up to 20-µm depth. Even though wide and shallow, pits are less dangerous than narrow and deep pits, which penetrate the material, and can cause stress peaks under load.

The passivation plateau for the same material (Mg10Gd2Nd in T4) exposed at 37°C starts at 1000 mV, see Figure 3(a). Repassivation exceeds 3000 mV. Therefore, at higher temperature repassivation due to more active microgalvanic corrosion was observed. The corroded surface in Figure 3(b) (top view) and the micrograph in Figure 4(b) (cross-section) present the corrosion attack after passing breakdown potential. Repassivation does not form a homogeneous oxide layer, which is impermeable to the electrolyte. The occurring repassivation even leads to the formation of elliptical and undercutting pits with a penetration depth up to 50 µm. Figure 4(b) also shows selective corrosion, where dendrite arms remained after heat treatment. Since the current density value at both temperatures is between 40 and 50 mA/cm^2 at 4000 mV, the material loss over all is assumed to be similar. Since undercutting pits cause high-stress peaks under load, they are not preferred.

3.3 Influence of heat treatment (T4/T6) on polarization curves

Since measurement at 37°C is similar to the human *in vivo* environment and due to increase in repassivation ability, the following are results from the measurements at 37°C. Table 1 shows that solution treatment T4 increased elongation at fracture by factor of 2: up to 7% for Mg10Gd1Nd-T4 and up to 3% for Mg10Gd2Nd-T4. Strength values did not change significantly after T4 compared with the as-cast alloys. Therefore, the as-cast condition of Mg10Gd*x*Nd has not been investigated further. However, Mg10Gd in as-cast was used as a reference for comparison in Figure 5(a) and 5(b) and does not show passivation; the corrosion current is constantly rising with increased potential. This behavior is contrary to the results obtained by Maier *et al.*[9] and explained by presence of flow and lower increase in pH value. Applying a flow rate leads to a stronger removal of corrosion products and therefore accelerates microgalvanic corrosion on the fresh metal surface. The repassivation behavior of the T6-treated Mg10Gd*x*Nd is better, see Figure 5(a) for Mg10Gd1Nd showing a small improvement and Figure 5(b) for Mg10Gd2Nd presenting a stronger repassivation, respectively. The current density is even found to decrease with increasing voltage for Mg10Gd2Nd. The shape of pitting corrosion is rated as subsurface and undercutting pitting and will be discussed in more detail in the Section 3.5.

The elongation at fracture of Mg10Gd1Nd in T4 condition presents the highest value, and repassivation, on the other hand, is less pronounced due to the absence of microgalvanic corrosion activity in the T4 condition. There is a difficult balance in the attempt to design a casting alloy based on Mg10Gd with sufficient mechanical properties and corrosion behavior. Stronger repassivation as a result of having precipitates with different electrode potentials to the α-matrix seems not to agree with the strong decrease in elongation at fracture due to precipitation hardening.

The presence of precipitate particles seems to assist in the passivation due to shorter galvanic pathways set up between the precipitates. The enhancement of the passivation behavior observed for the Mg10Gd2Nd alloy is attributed to the presence of finer scale β' precipitates observed in colonies in the alloy. Figure 2 compared with the Mg10Gd1Nd alloy. Further increase in the neodymium content or reducing the ratio between gadolinium and neodymium is expected to lead to better repassivation due to formation of fine distribution of precipitates.

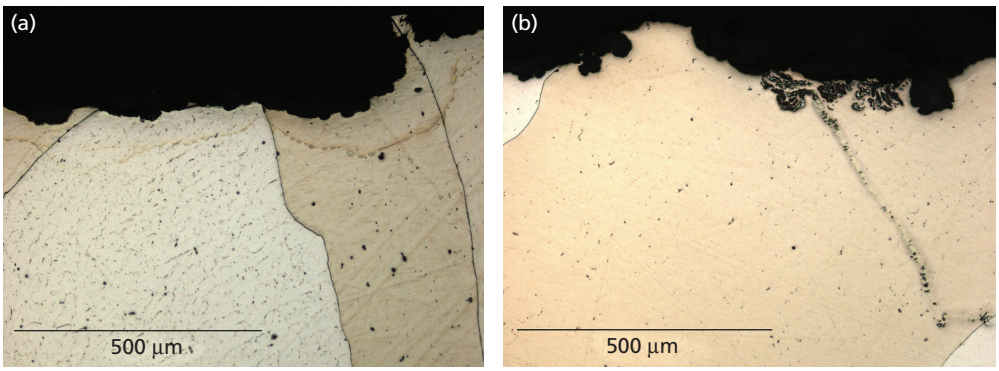

Figure 4. Microstructure of Mg10Gd2Nd-T4 after corrosion: (a) 22°C, wide and shallow pits, grain boundary acts as cathodic area and (b) 37°C, pitting corrosion in the shape of undercutting pits.

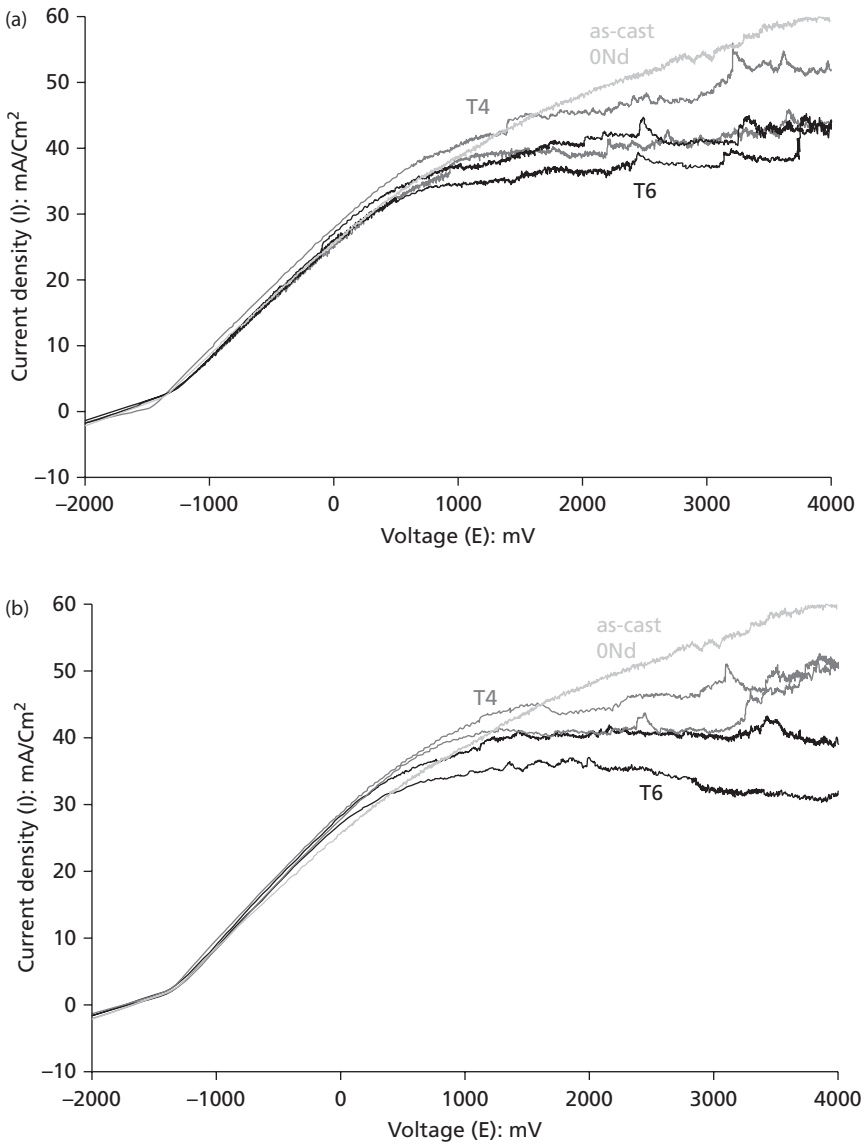

Figure 5. Potentiodynamic polarization curves (current density–potential (I–E) curves) at 37°C of (a) Mg10Gd1Nd and (b) Mg10Gd2Nd. Bright gray: as-cast Mg10Gd, gray: T4 and black: T6.

3.4 Influence of neodymium (1Nd/2Nd) on polarization curves

Figure 6(a) and 6(b) shows potentiodynamic polarization curves of Mg10Gd base alloy modified with 1 wt.% Nd and 2 wt.% Nd for T4 (Figure 6(a)) and T6 heat treatment (Figure 6(b)). There is no strong difference in corrosion in dependence of neodymium content in the T4 condition, since all precipitates should be dissolved during solution treatment. Within the active corrosion area, Mg10Gd2Nd shows a slight higher increase in corrosion current with increasing voltage. Here it is assumed that not all second-phase particles dissolves during T4 and a difference in electrode potential remains. In age hardened T6, Mg10Gd2Nd presents a reduction in corrosion current at the high-positive end of potential, see Figure 6b.

The passive/transpassive corrosion behavior of Mg10Gd1Nd-T4 alloy varies the most in Mg10Gd2Nd-T6 condition, which shows no breakdown potential before the potential of 4000 mV was reached. The duplex microstructure of coarse β_1-phase precipitates and regions containing much finer β'-phase precipitates promotes repassivation. The microgalvanic corrosion between these precipitates and the α-matrix allows the ongoing rebuilding of the passive oxide layer up to a high anodic corrosion exposure. However, the oxide film does not prevent further oxidation,

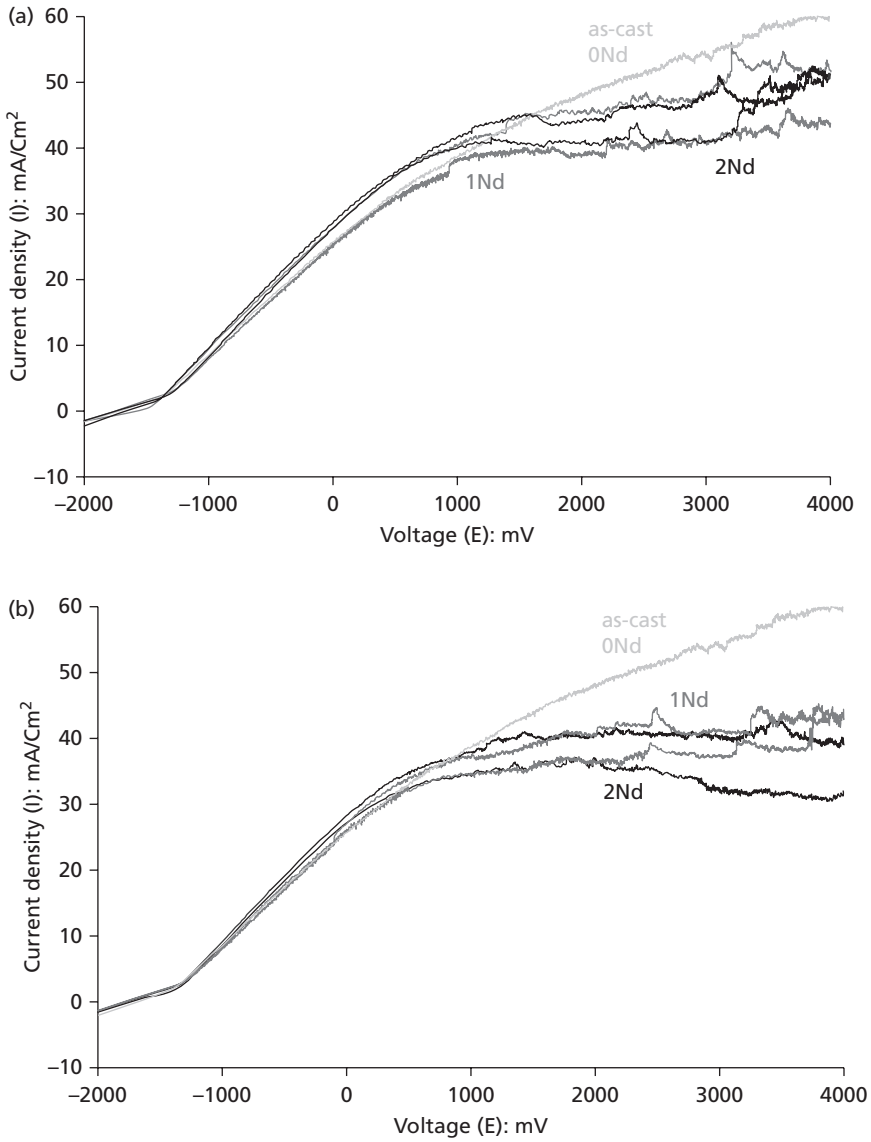

Figure 6. Potentiodynamic polarization curves (current density–potential (I–E) curves) at 37°C of (a) T4 and (b) T6. Bright gray: as-cast Mg10Gd, gray: Mg10Gd1Nd and black: Mg10Gd2Nd.

which will be seen discussing the cross-sectioned micrographs. Furthermore, this duplex microstructure leads to strong decrease in elongation at fracture. It is assumed that an elongation at fracture around 1% is too low and therefore, the material is too brittle for use as a medical implant material.

3.5 Influence of neodymium (1Nd/2Nd) and heat treatment (T4/T6) on shape of pitting corrosion

Figure 7(a)–7(d) shows cross-sectional micrographs of the corroded samples after reaching 4000 mV. The shape and size of pitting corrosion is discussed according the ASTM-G46-94 guidelines. Figure 7(a) shows the surface morphology of Mg10Gd1Nd-T4 after passing breakdown potential. Wide and shallow pits away from the grain boundary are observed. The tendency for undercutting pits is only found near grain boundaries, see left grain boundary in micrograph Figure 6(a).

Figure 7(b) presents the corrosion morphology of the Mg10Gd2Nd-T4 condition. The increase in neodymium content did not make a big difference on the potentiodynamic corrosion behavior. The cross-section also reveals wide and shallow pits changing into elliptical pits. As an example, micrograph surface pits are found for this material condition as a result of repassivation. However, the cross-section is taken after

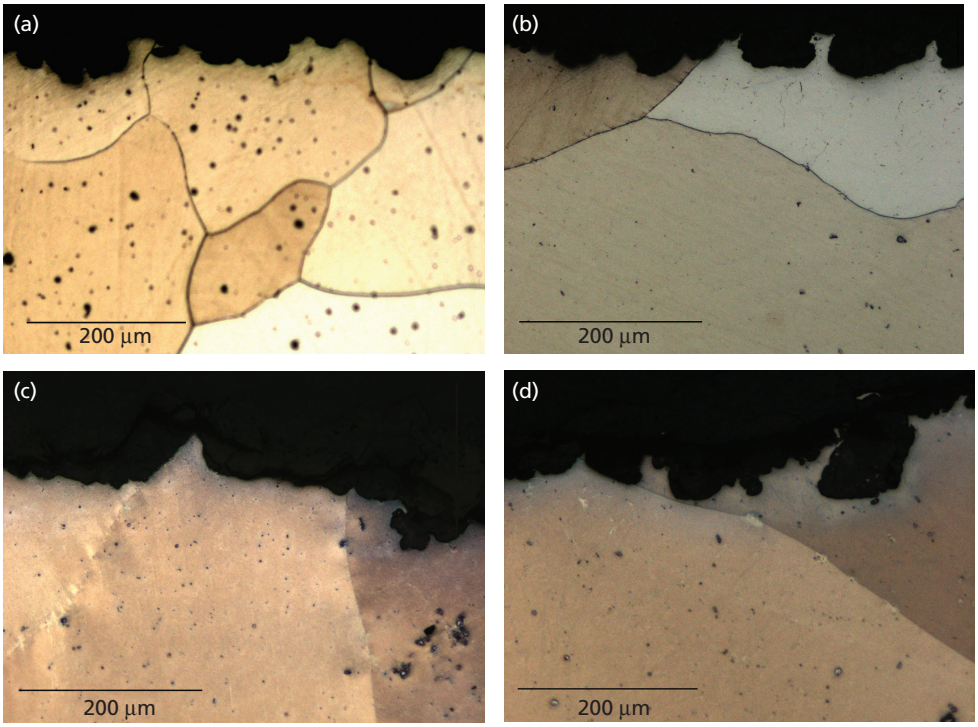

Figure 7. Microstructure of Mg10Gd*x*Nd after corrosion at 37°C of different neodymium contents and heat treatments: (a) Mg10Gd1Nd-T4, (b) Mg10Gd2Nd-T4, (c) Mg10Gd1Nd-T6 and (d) Mg10Gd2Nd-T6.

breakdown, so ongoing corrosion could change the morphology to wider and less deep pits. The cross-section of Mg10Gd1Nd-T6 in Figure 7(c) (before breakdown) presents undercutting pits, again, away from the grain boundary. Repassivation is present up to the end of the corrosion test, but the porosity of the oxide layer results in undercutting pits.

Figure 7(d) also shows a micrograph of Mg10Gd2Nd-T6 before breakdown. Strong subsurface pitting corrosion is seen. The formed oxide layer of this material (2 wt.% Nd and aged to peak hardened) repassivates the best, but contains a large number of pores. It can also be seen, that the grain boundary acts as the cathodic area with larger pits appearing further away from the boundary; intragranular corrosion is not present for these alloys. Electron microscopy images do not show extensive grain boundary precipitates, they were observed within the grains. There is no driving force caused by a sufficiently high electrode potential difference between second phases and α-matrix, as the binary Mg-10 wt% Gd alloy shows the lowest corrosion rate.[4]

4. Conclusion

An important issue for material development in medical applications is to meet the requirement specification of the magnesium alloys concerning corrosion rate and mechanical properties. The requirements of biodegradable metals depend on their application; it differs for human implantation such as bones (surgical application) or stents (cardiovascular treatments). With this work, it could be shown that by modifying the binary Mg-Gd alloy with an appropriate content of alloying elements, here neodymium, as well as the appropriate heat treatment, mechanical and corrosive properties can be adjusted. As-cast magnesium alloys fit to human bone properties regarding Young's modulus; however, they are lacking in ductility; the elongation at fracture is very low. Within the group of Mg-Gd-Nd alloys investigated in this study, Mg10Gd1Nd in T4 condition shows the highest value of elongation at fracture, up to 7% with moderate strength values. Strength, on the other hand, increases strongly due to precipitation hardening during isothermal aging (T6).

Potentiodynamic measurements were carried out with a three-electrode cell using Ringer acetate solution due to its similarity in human blood and applying a flow rate of 8 l/min to keep the pH value increase rather low. To fit the body temperature, measurements were taken at 37°C. The temperature increase from room temperature promotes microgalvanic corrosion, which depending on neodymium content and heat treatment improves

repassivation, even at very high anodic corrosion (up to 4000 mV). The alloys were stretched to pass breakdown potential. Isothermal aging (T6) improves repassivation, especially for Mg10Gd2Nd, where a duplex microstructure of coarse β_1-phase precipitates and regions containing much finer β' precipitates was found. In T4 condition, the content of neodymium does not influence the corrosion behavior. After the T6 heat treatment, the increase up to 2 wt.% Nd improves repassivation; breakdown potential could not be detected. However, as more active the repassivation is, more change the pitting corrosion results in wide and shallow pits forming the shape of undercutting and subsurface pits, which are expected to be more dangerous concerning stress peaks build up under load. Finally, as-cast binary Mg10Gd alloy does not show any passivation ability applying the flow cell; increasing the amount of neodymium as well as heat treatment, which in addition to solid solution and precipitation hardening also decreases the dendritic microstructure, is necessary.

Further work should concentrate on evaluating the electrochemical potential of the second phases itself, the matrix material surrounding these second phases and very local areas such as grain boundaries. With that the influence of the grain size on the corrosion behavior could be investigated in addition to chemical compositions and heat treatment. The complete picture will form by bringing the local electrochemical potential in correlation to its chemical composition. In this study, the temperature seems to influence the corrosion process the most, followed by the heat treatment and finally by the alloying composition (obviously depending on the Gd:Nd ratio). The mechanical properties, especially the strength, are also stronger, influenced by the heat treatment (an increase up to 150% in TYS for Mg10Gd2Nd in T6 condition) than by increasing neodymium content from 1 to 2 wt.%. Pitting corrosion to a different extent has been found in all investigated alloys using the flow cell influenced by the repassivation ability. The passive oxide layer reduces the corrosion rate in dependence on neodymium content and heat treatment. This result underlines the importance of understanding the formation of second phases and their influence on passivation. However, passive films should be stable, homogeneous and free of porosity. Cast Mg10Gd*x*Nd alloys seem to be susceptible to localized breakdown; resulting in accelerated corrosion of the underlying metal. Pitting corrosion is very dangerous when mechanical loading and corrosion take part simultaneously.

Acknowledgements

The authors appreciate the support of Gert Wiese (Helmholtz-Zentrum Geesthacht) with preparing samples for light microscopy and of Dipl.-Ing. (FH) Martin Wolf (Helmholtz-Zentrum Geesthacht) for determination of the dynamic modulus of elasticity using RFDA. The assistance of Hartmut Habeck Dipl.-Chem. (University of Applied Sciences Stralsund) during potentiodynamic polarization tests is also greatly appreciated.

REFERENCES

1. Witte, F. The history of biodegradable magnesium implants: a review. *Acta Biomaterialia* **2010**, *6*, 1680–1692.
2. Mueller, W.-D.; Nascimento, M. L.; Fernández Lorenzo de Mele, M. Critical discussion of the results from different corrosion studies of Mg and Mg alloys for biomaterial applications. *Acta Biomaterialia* **2010**, *6*, 1749–1755.
3. Witte, F.; Hort, N.; Vogt, C.; Cohen, S.; Kainer, K. U.; Feyerabend, F. Current developments in biodegradable magnesium. *Current Opinions in Solid State and Materials Science* **2008**, *12*, 63–72.
4. Hort, N.; Huang, Y.; Fechner, D.; Störmer, M.; Blawert, C.; Witte, F.; Vogt, C.; Drücker, H.; Willumeit, R.; Kainer, K. U.; Feyerabend, F. Magnesium alloys as implant materials – principles of property design for Mg-RE alloys. *Acta Biomaterialia* **2010**, *6*, 1714–1725.
5. Feyerabend, F.; Fischer, J.; Holtz, J.; Witte, F.; Willumeit, R.; Drücker, H.; Vogt, C.; Hort, N. Evaluation of short-term effects of rare earth and other elements used in magnesium alloys on primary cells and cell lines. *Acta Biomaterialia* **2010**, *6*, 1834–1842.
6. Apps, P. J.; Karimzadeh, H.; King, J. F.; Lorimer, G. W. Phase compositions in magnesium-rare earth alloys containing yttrium, gadolinium or dysprosium. *Scripta Materialia* **2003**, *48*, 475–481.
7. Apps, P. J.; Karimzadeh, H.; King, J. F.; Lorimer, G. W. Precipitation reactions in magnesium-rare alloys containing yttrium, gadolinium or dysprosium. *Scripta Materialia* **2003**, *48*, 1023–1028.
8. Nishijima, M.; Hiraga, K.; Yamasaki, M.; Kawamura, Y. Characterization of β' phase precipitates in an Mg-5 at% Gd alloy aged in a peak hardness condition, studied by high-angle annular detector dark-field scanning transmission electron microscopy. *Materials Transactions* **2006**, *47*, 2109–2112.
9. He, S. M.; Zeng, X. Q.; Peng, L. M.; Gao, X.; Nie, J. F.; Ding, W. J. Microstructure evolution in a Mg-15Gd-0.5Zr (wt%) alloy during isothermal aging at 250°C. *Material Science and Engineering A* **2006**, *431*, 322–327.
10. Vostry, P.; Smola, B.; Stukikova, I.; von Buch, F.; Mordike, B. L. Microstructure evolution in isochronally heat treated Mg-Gd alloys. *Physica Status Solidi A* **1999**, *175*, 491–500.
11. Maier, P.; Müller, S.; Dieringa, H.; Hort, N. Mechanical and corrosion properties of as-cast and extruded Mg10Gd alloy. In *Magnesium Technology 2012* (Mathaudhu, S. N.; Sillekens, W.; Hort, N.; Neelameggham, N. (eds.)). Hoboken: Wiley, 2012, 253–260.
12. Maier, P.; Tober, G.; Ruback, C.; Kuttig, M.; Anopuo, O.; Hort, N. Microstructural investigation on extruded Mg10Gd after exposure to fatigue and corrosion. In *Abstract Book 4th Symposium on Biodegradable Metals*, Italy, 2012, 16–18.

13. Elsayed, F. R.; Hort, N.; Salgado-Ordorica, M. A.; Kainer, K. U. Magnesium permanent mold casting optimization. *Materials Science Forum* **2011**, *690*, 65–68.
14. Salgado-Ordorica, M. A.; Punessen, W.; Yi, S.; Bohlen, J.; Kainer, K. U.; Hort, N. Macrostructure evolution in directionally solidified Mg-RE alloys. In *Magnesium Technology 2011* (Sillekens, W.; Agnew, S. R.; Neelameggham, N.; Mathaudhu, S. N. (eds.)). Hoboken: Wiley, 2011, 113–118.
15. Maier, P.; Richter, A.; Tober, T.; Hort, N. Effect of grain size and structure, solid solution elements, precipitates and twinning on nanohardness of Mg-RE alloys. *Materials Science Forum* **2013**, *765*, 491–495.
16. Zainal Abidin, N. I.; Atrens, A. D.; Martin, D.; Atrens, A. Corrosion of high purity Mg, Mg2Zn0.2Mn, ZE41 and AZ91 in Hank's solution at 37°C. *Corrosion Science* **2011**, *53*, 3542–355.